On Dynamic Channel Emulation in Sector MPAC for Over-the-Air Testing of Beamformed Massive MIMO Devices

Chen, Xiaochen ; Wang, Heng; Wang, Weimin ; Liu, Zheng; Liu, Yuanan

Published in:
China Communications

DOI (link to publication from Publisher):
10.23919/JCC.fa.2022-0644.202304

Publication date:
2023

Document Version
Accepted author manuscript, peer reviewed version

On Dynamic Channel Emulation in Sector MPAC for Over-the-Air Testing of Beamformed Massive MIMO Devices

Xiaochen Chen, Heng Wang, Zheng Liu, and Yuanan Liu

***Abstract*—In this article, novel emulation strategies for the sectored multiple probe anechoic chamber (SMPAC) are proposed to enable the reliable evaluation of the massive multiple-input multiple-output (MIMO) device operating at beamforming mode, which requires a realistic non-stationary channel environment. For the dynamic propagation emulation, an efficient closed-form probe weighting strategy minimizing the power angular spectrum (PAS) emulation errors is derived, substantially reducing the associated computational complexity. On the other hand, a novel probe selection algorithm is proposed to reproduce a more accurate fading environment. Various standard channel models and setup configurations are comprehensively simulated to validate the capacity of the proposed methods. The simulation results show that more competent active probes are selected with the proposed method compared to the conventional algorithms. Furthermore, the derived closed-form probe weighting strategy offers identical accuracy to that obtained with complicated numerical optimization. Moreover, a realistic dynamic channel measured in an indoor environment is reconstructed with the developed methodologies, and 95.6% PAS similarity can be achieved with 6 active probes. The satisfactory results demonstrate that the proposed algorithms are suitable for arbitrary channel emulation.**

***Index Terms*—Beamforming, channel emulation, massive MIMO device, multiple probe anechoic chamber (MPAC), over-the-air testing.**

I. Introduction

In recent years, to cope with the explosive growth of mobile data traffic driven by the increased wireless devices and applications, the fifth-generation (5G) wireless networks with ubiquitous, high-speed, low-latency, and reliable connectivity are under deployment. As the key 5G enabling component, massive multiple-input multiple-output (MIMO) technology is indispensable due to its capacity to further utilize the spatial resources [1]-[3] and the vast available spectral resources at the millimeter-wave (mm-wave) band [4]. Specifically, by establishing multiple narrow beams to deliver multiple data streams for multiple user terminals, the massive MIMO system is able to support multi-user (MU) MIMO communications over the same time-frequency resources in highly loaded cells without interference, improving the spectral efficiency [5]. On the other hand, the beamforming operation can offer a high array gain to compensate for the severe transmission losses at the mm-wave band [5]. Despite the great potential and promise of the massive MIMO system, many critical technical challenges remain to be addressed, and the feasibility in the real world requires careful verification [6]–[9]. For this reason, performance evaluation is of importance to help manufacturers identify design deficiencies and make well-directed rectifications to hardware and software designs in the early development phase. Unprecedented challenges, however, come to the beam-steerable massive MIMO systems. In beamforming working mode, both communication ends will steer the beam towards the optimal direction in the wireless link establishment process and keep the beams aligned in the time non-stationary channel environments caused by the mobility in one or both ends. Consequently, the realistic dynamic channel emulation is essential for the massive MIMO performance evaluation, while extensive efforts are mainly invested in the stationary channel emulation for the conventional user equipment (UE) testing [10].

Although it is essential to verify the device-under-test (DUT) in a realistic radio environment, the trials in a real word network, i.e., field trials, are generally undesirable since they are expensive, uncontrollable, unrepeatable, and time-consuming. Conducted testing in the laboratory was dominantly used by the industry due to its simplicity. However, since it is predicted that the massive MIMO DUT will not offer the antenna radio frequency (RF) connectors for testing, the conducted testing is impractical for the 5G new radio (NR) testing [11]. Therefore, the performance testing for the adaptive antenna systems will exclusively move to the radiated manners, i.e., so-called over-the-air (OTA) testing. OTA testing is a measurement methodology to assess the key performance indicators (KPIs) of the physically integrated DUT in normal working mode [12]. Strong efforts from industry and academia have been devoted to the OTA UE testing research [13]-[16], where the radiated two stages (RTS) methods and the multiple probe anechoic chamber (MPAC) for the 4G Long-Term Evolution (LTE) terminal testing was already selected and standardized by the Cellular Telecommunications and Internet Association (CTIA) and the Third Generation Partnership Project (3GPP) standards [17]. Nowadays, the standardization of the OTA verification methodology for 5G NR terminals is ongoing in 3GPP. The 3GPP TR 38.827 provided detailed specifications for the performance metrics, channel models, measurement methods, and verification procedures for the performance evaluation of 5G NR terminals [18]. MPAC is selected as the reference solution for 5G UE evaluation, while the RTS method can be adopted as well after the harmonization of measurement results with the MPAC solution [19]. More details about the standardization process and challenges of UE testing are discussed in [20].

While the standardization for 5G terminals is on its as-

cendant, the measurement methodology for massive MIMO base station (BS) is still under discussion. For the 5G beam-steerable massive MIMO testing, however, the RTS-based method is problematic, as it was not the real end-to-end testing [21]. The main drawback of RTS is that the antenna systems can not be adaptive (i.e., the beam-locked mode is required, and beamforming operations can not be tested). On the other hand, the exclusion of antenna effects is harmful to evaluating the wireless link performance of DUT [21]. Furthermore, from the views of the industry, the RTS method for massive MIMO requires large amounts of channel emulator (CE) resources, leading to cost-prohibitive setups [10].

MPAC is the real end-to-end testing method. In MPAC, the target channel modes can be mapped onto the probes deployed in the chamber. By appropriately controlling the excitation weights of probes, arbitrary propagation environments can be synthesized in the test zone with the help of CE. All critical parts (including the antenna effects) of the DUT can then be tested at once. It is technically sound for beam-steerable devices. In recent years, the industry and academia have been continuously focusing on studying the feasibility of the MPAC for massive MIMO BS. A cost-effective sectored MPAC (SMPAC) setup for the OTA testing of mm-wave massive MIMO device is proposed in [11]. References [22] and [23] offered systematic studies on SMPAC design, where the chamber configuration and performance metrics were discussed. To validate whether the channel environment is emulated in the practical MPAC setup as expected, efficient measurement methodologies are proposed in [19] [24]. A cost-effective switch matrix was designed in [25] for probe selection. To realize ultra-wideband channel emulation at the mm-wave band, [26] proposed a digital pre-distortion concept for the current CE. Reference [27] studied the performance degradation in SMPAC when the non-negligible mutual coupling between probes exists. To reduce hardware costs, [28] discussed a novel virtual MPAC solution for beam-steerable device evaluation. A comprehensive review of MPAC and SMPAC setup for OTA testing is detailed in [29]. Although many advanced SMAPC solutions have been proposed, there are still some issues that need to be addressed. The limitations can be summarized as follows:

- It is recognized that the adaptive beamforming systems operate in non-stationary (time-variant) propagation scenarios and will dynamically change their beams according to the estimated channel state information (CSI) [30]. It can be expected that realistic dynamic propagation emulation is necessitated to reflect the exact performance of the beam-steerable DUT. Accurate channel emulation for the large aperture DUT with high spatial resolution, however, necessitates a high number of probes and the associated hardware resources. Since the channels are generally directive and sparse at the mm-wave band, the probe selection algorithm is capable of reducing the hardware requirement. Compared to the stationary channel scenarios, the probe selection algorithm for the massive MIMO testing should not only be competent enough for the need for synthesizing accurate channels but also be computationally efficient to meet the need for dynamic emulation. However, the conventional high-performance probe selection algorithms are too time-consuming, such as the particle swarm optimization (PSO) method [31] and the brute force method [32].
- For 4G LTE UE testing, spatial correlation [10] is generally used as the metric for probe weighting computation. However, the spatial correlation becomes less relevant to the massive MIMO testing [11]. As discussed in [30], beamforming operations highly rely on propagation path information rather than statistical characteristics. Furthermore, different power angular spectrums (PASs) may yield similar spatial correlation, which is always high at the mm-wave band due to the narrow path angular spread. Reference [33] proposed an effective PAS reconstruction error-based probe weighting strategy. However, it requires complicated numerical optimization to solve the objective function and is not suitable for dynamic channel emulation.
- One of the key factors of the high costs of SMPAC is that the chamber dimension should be large enough to satisfy the far-field criterion for DUT [23]. [23] studied the near-field effects on emulation accuracy, while the compensation methods were not given.

This paper aims to provide a novel SMPAC configuration methodology to enable efficient massive MIMO verification in the small chamber. To tackle the above limitations, the main contributions of this paper are threefold:

1) The probe weighting strategy based on minimizing the PAS reconstruction error is analytically derived, and a closed-form solution is then obtained. Thus for dynamic channel emulation, the calculations for probe weights can be implemented with low computational complexity.
2) A novel probe selection algorithm called the backward verified orthogonal matching pursuit (BVOMP) method is proposed, coordinating the accuracy and computational complexity. With the proposed closed-form probe weighting strategy, the probe selection can be performed efficiently. The obtained active probes can emulate the target channel more accurately for the massive MIMO testing compared to the other low-complexity algorithms. Furthermore, the phase distortions, in near-field measurement, are considered in the proposed probe selection method, improving the emulation accuracy in the small chamber.
3) Comprehensive studies on the setup configurations, including the chamber dimension, the probe spacing, and the number of active probes, are performed to find the cost-effective design parameters. In addition to various standard channels, a realistic measured channel is used to validate the effectiveness of the proposed methodology. It proves that arbitrary propagation channels can be emulated with the proposed SMPAC solution.

This research focus of this paper is on the single snapshot channel emulation since the extension to the multi-snapshot channel can be straightforwardly implemented by repeating

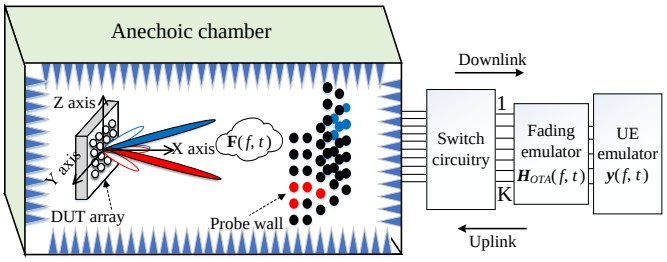

Fig. 1. The diagram of the MPAC setup.

the proposed methodology and interpolation algorithm. The procedures of multi-snapshot extension are detailed in [34].

The rest of the paper is arranged as follows. Section II elaborates on the SMPAC components, system models of the radio channel and the OTA setup, and the conventional channel emulation method. In Section III, important state-of-the-art probe selection and weighting algorithms are discussed, followed by the proposed strategies. Comprehensive numerical analyses are provided in Section IV, where various setup designs are considered. The conclusions are drawn in Section V.

II. System Model

In this section, we first outline the principle and the signal model of the SMPAC setup. Then the general OTA emulation method based on spatial correlation metric is briefly revisited.

A. MPAC Setup

It is recognized that three-dimensional (3-D) MIMO (in azimuth and elevation) is employed to further utilize the spatial resource and enhance the beamforming capacity in 5G NR. To realize 3-D propagation channel emulation, a large set of OTA probes covering the sector of interest with certain angle spacing are deployed in the anechoic chamber, where the distances from the probes to the center of DUT are approximately the same. The sector design is based on the fact that, for most scenarios, the angular power distribution of the channel seen by the BS is confined in a limited angle region [11], reducing hardware costs. The SMPAC setup is composed of an anechoic chamber, a carefully designed probe wall, switching circuitry, a CE, and a UE emulator, as shown in Fig. 1. In the following, the underlying principle for SMPAC emulation is illustrated with the uplink transmission (from the user side to the BS side) as an example. The UE emulator creates the testing signal as transmit (Tx) signal, which is then fed to the CE. The CE generates the channel impulse responses (CIR) containing specific channel characteristics, such as Doppler spectrum, Power Delay Profile (PDP), UE side effects, Cross Polarization Ratio (XPR), fast fading, and noises. Then the Tx signals are convolved with the generated CIRs and then radiated from the probes. To accurately emulate the spatial profiles of the target propagation channels at the DUT side, the active probes should be appropriately selected and excited. To sum up, the purpose of this setup is to synthesize a desired time-variant electromagnetic environment around the DUT by properly setting the generated CIRs in CE and the probe weights according to the employed probe configuration and the target channel model. In this way, the DUT operates normally as in the intended scenario, but in a controllable laboratory environment.

B. Signal Model

Th well-known MIMO communication signal model (neglecting noise) can be expressed as:

$$\boldsymbol{y}(f,t) = \mathbf{H}(f,t)\boldsymbol{x}(f,t), \tag{1}$$

where $y(f,t) \in \mathbb{C}^{N\times 1}$ and $x(f,t) \in \mathbb{C}^{D\times 1}$ are the receive (Rx) and the Tx signal vectors, respectively. N and D denote the numbers of the antenna elements contained in the receiver (BS) and transmitter (UE, single-user case). $\mathbf{H}(f,t) \in \mathbb{C}^{N\times D}$ is the transfer matrix in real propagation. t and f mean the time and frequency.

In SMPAC, the signal model is substituted by:

$$\boldsymbol{y}(f,t) = \mathbf{F}(f,t)\mathbf{H}_{OTA}(f,t)\boldsymbol{x}(f,t), \tag{2}$$

$\mathbf{H}_{OTA} \in \mathbb{C}^{K\times D}(f,t)$ is the channel matrix, including the CIRs generated in CE for the K active probes. $\boldsymbol{F}(f,t) = \{\gamma_{n,k}\} \in \mathbb{C}^{N\times K}$ is the transfer matrix between the K active probes and the DUT. Ideally, the objective of channel emulation is to realize $\mathbf{F}\mathbf{H}_{OTA} = \mathbf{H}$ by properly designing $\mathbf{H}_{OTA}$. Theoretically, one can simply specify it as:

$$\mathbf{H}_{OTA} = \mathbf{F}^{-1}\mathbf{H}. \tag{3}$$

However, it is impractical since $\mathbf{F}$ is typically non-measurable [22]. Thus, the main emulation challenge is how to reproduce the spatial characteristics of the target channel with the given probe configuration, while the other channel characteristics (e.g., temporal, frequency, polarization, and fading) can be easily implemented in CE. To this end, the emulation principle based on the statistical spatial correlation is introduced in the following.

C. Channel Emulation

Generally speaking, there are two emulation approaches that can be applied for reconstructing the target spatial profiles, i.e., the prefaded synthesis (PFS) and the plane-wave synthesis (PWS). It has been concluded in [22] that PFS is more suitable for the SMPAC emulation, while PWS suffers from the problems of high cost and strict phase coherence. Thus PFS technique is exploited in this work.

Based on the wide-sense stationary uncorrelated scattering (WSSUS) assumption [35] at each channel snapshot, the spatial channel can be fully characterized and emulated with the second-order statistics, i.e., the spatial correlation. Specifically, for the target far-field channel PAS $P(\Omega)$, the spatial correlation of which between the uth and the vth DUT antenna elements can be formatted as [10]:

$$\rho_{u,v} = \oint P(\Omega)\exp(j\boldsymbol{\beta}_\Omega(\boldsymbol{r}_u - \boldsymbol{r}_v))d\Omega, \tag{4}$$

where $\boldsymbol{r}_u$ and $\boldsymbol{r}_v$ represent the location vectors of the uth and the vth DUT antennas. $\boldsymbol{\beta}_\Omega$ is the wave vector defined by the frequency and the direction of the solid angle Ω. Considering

the near-field effects, the spatial correlation emulated with K probes can be expressed as [22]:

$$\hat{\rho}_{u,v} = \frac{\sum_{k=1}^{K} g_k L(d_{k,u}) L(d_{k,v}) \exp(j\,||\boldsymbol{\beta}_\Omega||\,(d_{k,v} - d_{k,u}))}{\sqrt{\sum_{k=1}^{K} g_k L^2(d_{k,u}) \sum_{k=1}^{K} g_k L^2(d_{k,v})}}, \tag{5}$$

where g_k is the power weight for the kth active probe. $d_{k,u}$ and $L^2(d_{k,u})$ are the distance and path loss between the kth active probe and the uth DUT antenna. An objective function can be constructed and then applied to optimize the probe weights:

$$\boldsymbol{g} = \arg\min_{\boldsymbol{g}} \parallel \hat{\boldsymbol{\rho}} - \boldsymbol{\rho} \parallel_2^2. \tag{6}$$

$\boldsymbol{\rho} = \{\rho_{u,v}\}$ and $\hat{\boldsymbol{\rho}} = \{\hat{\rho}_{u,v}\}$ are the target and the emulated channel spatial correlation vectors, respectively, for all combinations of antenna pairs. $\boldsymbol{g} = \{g_k\} \in \mathbb{C}^{K\times 1}$ is the vector that contains the power weights for the K active probes. $\|\cdot\|_2$ is the 2-norm computation. (6) can be solved by convex optimization [10].

Based on equations (4)-(6), it can be found that the probe weights, together with the locations, jointly determine the emulated environment. Since the hardware resources are limited, not all probes can be simultaneously excited. Therefore, a sophisticated probe selection algorithm is required to realize the satisfying channel emulation for the massive MIMO DUT verifications. On the other hand, the channel emulation minimizing the spatial correlation errors limits the capacity to reflect the array features of DUT, while the emulation based on PAS reconstruction errors is more competent for the massive MIMO OTA testing. Moreover, to satisfy the requirements for dynamic (non-stationary) channel emulation, the probe weight calculation should be computationally efficient, and the numerical computation with convex optimization is unsuitable. In the following, a high-performance probe allocation methodology and a closed-form probe weighting strategy minimizing the PAS reconstruction errors are proposed.

III. Probe Selection and Weighting Algorithm

A. Existing Algorithm

1) Power weighting method: For most MPAC research, the optimal probe weights are calculated with spatial correlation, e.g., by minimizing the maximum correlation error or mean correlation error [36]. [21] proposed a power weighting strategy based on the Bartlett beamformer. Though computationally efficient, it offers limited emulation accuracy due to the sidelobe effects caused by the underlying mechanism. The direct sampling method discussed in [22] suffers from the accuracy problem as well. By minimizing the PAS reconstruction errors with convex optimization, reference [33] proposed a power weighting method exhibiting satisfying PAS emulation accuracy, which is critical for testing the massive MIMO DUT with high spatial resolution. The problem with this method is that the computational complexity is too high for dynamic channel reconstruction. In this work, we aim to derive a novel closed-form probe weighting method minimizing the reconstructed PAS errors, providing identical accuracy to that obtained with the convex optimization in far-field conditions.

2) Probe Selection Method: Many probe selection algorithms have been proposed for the conventional two-dimensional (2-D) MAPC setup and are mainly for stationary channel emulation [31] [32]. The common challenge of them lies in the computational complexity of emulating the dynamic propagations. For instance, the multi-shot algorithm [32] demands multiple high-dimensional convex optimizations due to a large number of available probes, and the PSO algorithm [31] requires even more computing time. [37] proposed a forward allocation (FA) algorithm based on the orthogonal matching pursuit (OMP) principle [38]. Though only correlation computation and low-dimensional convex optimizations are required, the emulation accuracy should be further improved for beamforming technology verifications. Also, a simple spatial angle mapping (SAM) method was proposed in [22] and has been widely adopted in the literature [11] [21]. The main disadvantages are that it offers limited emulation accuracy and can only be applied to cluster-based channels.

B. Probe Weighing Strategy

According to the Bartlett beamformer [39], the PAS estimated (seen) by the DUT in ideal and OTA cases can be formatted as:

$$\hat{P}_T(\Omega) = \boldsymbol{a}^H(\Omega)\boldsymbol{R}\boldsymbol{a}(\Omega) \tag{7}$$

$$\hat{P}_O(\Omega) = \boldsymbol{a}^H(\Omega)\hat{\boldsymbol{R}}\boldsymbol{a}(\Omega) \tag{8}$$

$\boldsymbol{R}$ and $\hat{\boldsymbol{R}}$ are the spatial correlation matrix. $\boldsymbol{a}(\Omega) = [a_1(\Omega), a_2(\Omega), ..., a_N(\Omega)] \in \mathbb{C}^{N\times 1}$ is the array steering vector of the DUT and can be expressed as:

$$a_n(\Omega) = \exp(j\boldsymbol{\beta}_\Omega \boldsymbol{r}_n), \tag{9}$$

we first derive the PAS estimated by the DUT in OTA cases with the analytical formulation. For a DUT composed of N antenna elements, the emulated spatial correlation matrix can be constructed as:

$$\hat{\mathbf{R}} = \begin{bmatrix} \overline{\rho}_{1,1} & \cdots & \overline{\rho}_{1,N} \\ \overline{\rho}_{2,1} & \cdots & \overline{\rho}_{2,N} \\ \vdots & \ddots & \vdots \\ \overline{\rho}_{N,1} & \cdots & \overline{\rho}_{N,N} \end{bmatrix}, \tag{10}$$

where $\overline{\rho}_{u,v}$ is the emulated spatial correlation in simplified form and can be expressed as:

$$\overline{\rho}_{u,v} = \sum_{k=1}^{K} g_k L(d_{k,u}) L(d_{k,v}) \exp(j\,||\boldsymbol{\beta}_\Omega||\,(d_{k,v} - d_{k,u})), \tag{11}$$

It can be found that the denominator in equation (5) is omitted here. The operation is based on two facts: First, in far-field conditions, the denominator in equation (5) equals 1 [10], and the omission will not cause inaccuracy. Secondly, the denominator in equation (5) is used to characterize the distortions of the magnitude field on the DUT plane caused by the path loss in near-field conditions. However, it is less significant, while phase distortions play critical roles in channel emulation. Thus we remove the denominator of equation (5) for simplicity. The

effectiveness will be demonstrated in the simulation section. Then perform the flowing operation:

$$\boldsymbol{a}^H(\Omega)\hat{\mathbf{R}} = \left[\sum_{n=1}^{N}\exp(-j\boldsymbol{\beta}_\Omega \boldsymbol{r}_n)\overline{\rho}_{n,1}, \sum_{n=1}^{N}\exp(-j\boldsymbol{\beta}_\Omega \boldsymbol{r}_n)\overline{\rho}_{n,2}, ..., \sum_{n=1}^{N}\exp(-j\boldsymbol{\beta}_\Omega \boldsymbol{r}_n)\overline{\rho}_{n,N}\right] = [W'_1, W'_2, ..., W'_N] \in \mathbb{C}^{1\times N} \tag{12}$$

where $W'_{n'}$ can be formulated as:

$$W'_{n'} = \sum_{n=1}^{N}\sum_{k=1}^{K} g_k L(d_{k,n'})L(d_{k,n})\exp(j\,||\boldsymbol{\beta}_\Omega||\,(d_{k,n'} - d_{k,n} - \frac{\boldsymbol{\beta}_\Omega \boldsymbol{r}_n}{||\boldsymbol{\beta}_\Omega||})). \tag{13}$$

After multiplying the equation (12) by $\boldsymbol{a}(\Omega)$:

$$\begin{aligned}\boldsymbol{a}^H(\Omega)\hat{\mathbf{R}}\boldsymbol{a}(\Omega) &= \sum_{n'=1}^{N} W'_{n'}\exp(j\boldsymbol{\beta}_\Omega \boldsymbol{r}'_n) \\ &= \sum_{n'=1}^{N}\sum_{n=1}^{N}\sum_{k=1}^{K} g_k L(d_{k,n'})L(d_{k,n}) \\ &\quad \cdot \exp(j\,||\boldsymbol{\beta}_\Omega||\,(d_{k,n'} - d_{k,n} - \frac{\boldsymbol{\beta}_\Omega \boldsymbol{r}_n}{||\boldsymbol{\beta}_\Omega||} + \frac{\boldsymbol{\beta}_\Omega \boldsymbol{r}_{n'}}{||\boldsymbol{\beta}_\Omega||})).\end{aligned} \tag{14}$$

It is observed that equation (14) can be rewritten as:

$$\boldsymbol{a}^H(\Omega)\hat{\mathbf{R}}\boldsymbol{a}(\Omega) = [\widetilde{W}_1(\Omega), \widetilde{W}_2(\Omega), ..., \widetilde{W}_K(\Omega)] \cdot \begin{bmatrix} g_1 \\ g_2 \\ \vdots \\ g_K \end{bmatrix} \tag{15}$$

where

$$\begin{aligned}\widetilde{W}_k(\Omega) &= \sum_{n'=1}^{N}\sum_{n=1}^{N} L(d_{k,n'})L(d_{k,n}) \\ &\quad \cdot \exp(j\,||\boldsymbol{\beta}_\Omega||\,(d_{k,n'} - d_{k,n} - \frac{\boldsymbol{\beta}_\Omega \boldsymbol{r}_n}{||\boldsymbol{\beta}_\Omega||} + \frac{\boldsymbol{\beta}_\Omega \boldsymbol{r}_{n'}}{||\boldsymbol{\beta}_\Omega||})).\end{aligned} \tag{16}$$

An analytical expression of $\hat{P}_O$ is obtained for a given space angle Ω. Then we can obtain vector $\hat{\boldsymbol{P}}_O = [\hat{P}_O(\Omega_1), \hat{P}_O(\Omega_2), ..., \hat{P}_O(\Omega_Q)]$ composed of the estimated PAS for all space angles of interest. $\hat{\boldsymbol{P}}_O$ can be transformed into the form of a regression equation:

$$\underbrace{\begin{bmatrix} \widetilde{W}_1(\Omega_1), \widetilde{W}_2(\Omega_1) & \cdots & \widetilde{W}_K(\Omega_1) \\ \widetilde{W}_1(\Omega_2), \widetilde{W}_2(\Omega_2) & \cdots & \widetilde{W}_K(\Omega_2) \\ \vdots \quad \vdots & \ddots & \vdots \\ \widetilde{W}_1(\Omega_Q), \widetilde{W}_2(\Omega_Q) & \cdots & \widetilde{W}_K(\Omega_Q) \end{bmatrix}}_{\widetilde{\mathbf{W}}} \cdot \underbrace{\begin{bmatrix} g_1 \\ g_2 \\ \vdots \\ g_K \end{bmatrix}}_{\boldsymbol{g}} = \underbrace{\begin{bmatrix} \hat{P}_O(\Omega_1) \\ \hat{P}_O(\Omega_2) \\ \vdots \\ \hat{P}_O(\Omega_Q) \end{bmatrix}}_{\hat{\boldsymbol{P}}_O}, \tag{17}$$

$\widetilde{\mathbf{W}} \in \mathbb{C}^{Q\times K}$ is the matrix characterizing the contributions of the K probes in synthesizing the emulated PAS and is called the feature matrix in this paper. The probe power weights minimizing the PAS reconstruction errors can be expressed as:

$$\boldsymbol{g} = \arg\min_{\boldsymbol{g}} \| \widetilde{\mathbf{W}}\boldsymbol{g} - \boldsymbol{P}_T \|_2^2. \tag{18}$$

where $\boldsymbol{P}_T = [\hat{P}_T(\Omega_1), \hat{P}_T(\Omega_2), ..., \hat{P}_T(\Omega_Q)]$. Different from the spatial correlation calculation, the elements in $\widetilde{\mathbf{W}}$ are real numbers due to the symmetric calculation in equation (16). Also the elements in $\boldsymbol{g}$ and $\boldsymbol{P}_T$ are real numbers. Thus we can directly employ the Least Square Method (LMS) [40] to solve this linear regression problem. The probe weights can be calculated as:

$$\boldsymbol{g} = (\widetilde{\mathbf{W}}^T \cdot \widetilde{\mathbf{W}})^{-1} \cdot \widetilde{\mathbf{W}}^T \cdot \boldsymbol{P}_T. \tag{19}$$

$(\cdot)^T$ is the transpose operation. Though computationally simple, the probe weights with (19) do not satisfy the constraint of $\| \boldsymbol{g}\|_1 = 1$ in a practical SMPAC setup, where $\|\cdot\|_1$ represents the 1-norm operation. To enable the probe weights to minimize the PAS reconstruction errors and satisfy the constraint, a new objective function is constructed:

$$\begin{aligned}\boldsymbol{\Delta} &= \|\widetilde{\boldsymbol{W}}\boldsymbol{g} - \boldsymbol{P}_T\|_2^2 + \alpha(\|\boldsymbol{g}\|_1 - 1) \\ &= (\widetilde{\mathbf{W}}\boldsymbol{g} - \boldsymbol{P}_T) \cdot (\widetilde{\mathbf{W}}\boldsymbol{g} - \boldsymbol{P}_T)^T + \alpha(\|\boldsymbol{g}\|_1 - 1),\end{aligned} \tag{20}$$

α is a hyper-parameter. Take the partial derivatives of $\boldsymbol{\Delta}$, and they should satisfy:

$$\begin{cases} \frac{\partial \boldsymbol{\Delta}}{\partial \boldsymbol{g}} = 0 \\ \frac{\partial \boldsymbol{\Delta}}{\partial \alpha} = 0 \end{cases}. \tag{21}$$

With (21), the optimal probe weights and the suitable hyper-parameter can be computed as:

$$\boldsymbol{g}_{opt} = (\widetilde{\mathbf{W}}^T \cdot \widetilde{\mathbf{W}})^{-1} \cdot (\widetilde{\mathbf{W}}^T \cdot \boldsymbol{P}_T - \frac{\alpha \boldsymbol{I}}{2}), \tag{22}$$

$$\alpha_{opt} = \frac{2 \cdot \boldsymbol{I}^T(\widetilde{\mathbf{W}}^T \cdot \widetilde{\mathbf{W}})^{-1}(\widetilde{\mathbf{W}}^T \cdot \boldsymbol{P}_T) - 2}{\boldsymbol{I}^T(\widetilde{\mathbf{W}}^T \cdot \widetilde{\mathbf{W}})^{-1}\boldsymbol{I}}, \tag{23}$$

where $\boldsymbol{I} = [1, ...1]^T \in \mathbb{C}^{K\times 1}$ is a unit column vector. According to the Lagrange multiplier mechanism [40], $\boldsymbol{g}_{opt}$ with α_{opt} is the optimal solution for minimizing the PAS reconstruction errors with the constraint of $\|\boldsymbol{g}\|_1 = 1$. Obviously, (19), (22), and (23) are closed-form expressions and can offer low computational complexity for the following probe selection algorithm. Note that if the optimal weight of a specific probe is smaller than 0, it means that this probe can not contribute to the emulation, and its weight should be forcedly set to 0.

C. Probe Selection Strategy

To accurately reproduce the PAS profile for the beam-steerable DUT with the limited numbers (generally no more than 16) of active probes, a novel BVOMP algorithm is developed, where an adaptive correction procedure is introduced for the OMP mechanism. It should be stressed that there is no need for numerical optimization in this section, and all procedures can be implemented with the derived closed-form solutions, i.e., (19), (22), and (23). Specifically, we first construct a dictionary $\widetilde{\mathbf{W}}' = \left[\widetilde{\boldsymbol{W}}_1, \widetilde{\boldsymbol{W}}_2, ..., \widetilde{\boldsymbol{W}}_M\right] \in \mathbb{C}^{Q\times M}$

for all M available probes, where the column vector is called the feature vector in the following, and the mth column vector $\widetilde{\boldsymbol{W}}_m = [\widetilde{W}_m(\Omega_1), \widetilde{W}_m(\Omega_2), ..., \widetilde{W}_m(\Omega_Q)] \in \mathbb{C}^{Q\times 1}$ represents the partial PAS reconstructed by the mth available probe. According to the contributions of all available probes in emulating the desired PAS, a probe set can be selected with the OMP principle. Finally, the adaptive correction is implemented for the selected probes to find the optimal probe set. The specific procedures can be summarized as follows:

1) Using (4) and (7), calculate the PAS $\boldsymbol{P}_T$ estimated by DUT in the target channel environment. For the given probe configuration, construct the dictionary $\widetilde{\mathbf{W}}'$ based on (16). $s = 1$. Define $\widetilde{\mathbf{W}}_s^{sel} = \boldsymbol{\phi}$ and the current residual PAS $\boldsymbol{r}_s = \boldsymbol{P}_T$. $l = 1$.
2) Calculate the correlation coefficients between $\boldsymbol{r}_s$ and all the feature vectors in $\widetilde{\mathbf{W}}'$. The available probe with the maximum positive correlation coefficient is selected, and the corresponding feature vector is added to $\widetilde{\mathbf{W}}_s^{sel}$. Using (19), calculate the power weights for the s selected probes.
3) Update residual $\boldsymbol{r}_{s+1} = \boldsymbol{P}_T - \widetilde{\mathbf{W}}_s^{sel}\boldsymbol{g}$, and $s = s + 1$.
4) Repeat procedures 2-3 until K probes are determined.
5) Calculate the power weights $\boldsymbol{g}_{opt}$ for the K selected probes with (22) and (23). The emulation error is $\overline{\delta} = \|\boldsymbol{P}_T - \widetilde{\mathbf{W}}_s^{sel}\boldsymbol{g}_{opt}\|_2$.
6) The $M-K$ unselected probes are respectively combined with the already selected probes except for the lth selected probe, and therefore $M - K$ temporary feature matrices are obtained. The temporary feature matrix is denoted by $\overline{\mathbf{W}}$. Calculate the power weights $\boldsymbol{g}_{opt}$ for the $M - K$ temporary feature matrices with (22) and (23), and the $M - K$ emulation errors are therefore obtained. Among the $M - K$ emulation errors, if the minimum value δ' is smaller than $\overline{\delta}$, the lth selected probe is replaced by the unselected probe corresponding to the temporary feature matrix providing the emulation error δ'. $l = l+1$ and $\overline{\delta} = \delta'$. Repeat this procedure to examine all the selected probes.
7) $l = 1$, and repeat procedure 6 until $\overline{\delta}$ does not change.

Procedure 6 is the so-called adaptive correction. Since the OMP method is a greedy algorithm aiming for the local optimum, the already selected probes may no longer contribute the most to the emulation after new probes are determined, limiting the emulation accuracy. For this reason, adaptive correction is introduced to adjust the selected probes for more realistic PAS reconstruction for the massive MIMO DUT testing. Though more computations are required, the closed-form probe weighting strategy ensures low complexity. The framework of the proposed selection method is summarized in Algorithm 1, which is the most general and complete case. Actually, the adaptive correction can be performed only once since the second time correction provides limited improvement. Furthermore, not all of these $M - K$ probes should be considered in the adaptive correction procedure since the possible optimal probe is located around the examined probe. It is beneficial to develop a guideline to restrict the selection region in the correction procedure, which is our further research.

Algorithm 1: BVOMP algorithm

Input: K, $\boldsymbol{P}_T$, and dictionary $\widetilde{\mathbf{W}}'$.
initialization: Initial residual PAS: $\boldsymbol{r}_1 = \boldsymbol{P}_T$. Define $s = 1$, $\widetilde{\mathbf{W}}_s^{sel} = \boldsymbol{\phi}$, $l = 1$, $\tau = 1$, $\delta_0 = +\infty$;
while $s \le K$ **do**
  Select the m^{sel}th probe presenting maximum positive correlation with $\boldsymbol{r}_s$

$$m^{sel} = \arg\max_m \left\{ \frac{\sum_{q=1}^{Q} \widetilde{\boldsymbol{W}}_m^*(\Omega_q)\cdot \boldsymbol{r}_s(\Omega_q)}{\sqrt{\sum_{q=1}^{Q} \widetilde{\boldsymbol{W}}_m^*(\Omega_q)\cdot \widetilde{\boldsymbol{W}}_m(\Omega_q)}} \middle| \widetilde{\boldsymbol{W}}_m \in \widetilde{\mathbf{W}}' \right\}$$

  Update $\widetilde{\mathbf{W}}_s^{sel}$ and calculate the power weights with (19);
  Update $\boldsymbol{r}_{s+1} = \boldsymbol{P}_T - \widetilde{\mathbf{W}}_s^{sel}\boldsymbol{g}$, and $s = s + 1$.;
end
$\delta_\tau = \overline{\delta} = \|\boldsymbol{P}_T - \widetilde{\mathbf{W}}_s^{sel}\boldsymbol{g}_{opt}\|_2$;
while $\delta_\tau < \delta_{\tau-1}$ **do**
  for $l = 1$ *to* K **do**
    for $c = 1$ *to* $M - K$ **do**
      Combine the cth unselected probe with the already selected probes except for the lth selected probe to construct the temporary feature matrix $\overline{\mathbf{W}}$.
      Calculate the current emulation error: $\boldsymbol{\delta}(c) = \|\boldsymbol{P}_T - \overline{\mathbf{W}}\boldsymbol{g}_{opt}\|_2$, where the optimal power weights are obtained with (22) and (23).
    end
    $\delta' = \min(\boldsymbol{\delta})$.
    if $\delta' < \overline{\delta}$ **then**
      Replace the lth selected probe with the unselected probe presenting δ'. $\overline{\delta} = \delta'$.
    end
  end
  $\delta_\tau = \overline{\delta}$, $\tau = \tau + 1$.
end
Output: K selected probes.

IV. Algorithm Validation

This section comprehensively investigates the performances of our proposed methodologies in propagation emulation with different setup configurations. Four popular algorithm combinations, as shown in Table. I, are implemented for comparison, where B5 offers the most realistic channel emulation that can be achieved with the given setup. An 8×8 array with half-wavelength spacing is assumed to be the DUT. Since the sub-6 GHz DUT requires more demanding far-field conditions [23], 3.5 GHz is set to be the carrier frequency for examining the robustness of our proposed algorithms in near-field conditions. Note that the mm-wave band can be emulated with the

TABLE I
ALGORITHM COMBINATION.

configuration	Probe selection	Probe weighting
B1	SAM [22]	spatial correlation method with numerical optimization [10]
B2	SAM [22]	proposed method
B3	OMP [37]	proposed method
B4	proposed BVOMP	proposed method
B5	All probes work	PAS reconstruction error with numerical optimization [33]

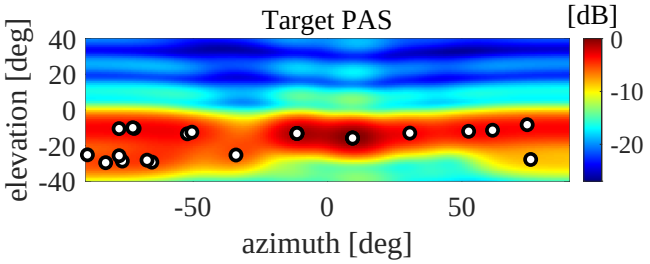

Fig. 2. Estimated PAS of the CDL-B channel model in the target environment.

proposed methods as well. The widely used four metrics [22], i.e., the PAS similarity, the weighted root mean square (RMS) spatial correlation error e_ρ, the beam peak distance D_P, and the total variation distance of beam allocations D_T, are adopted in this section to evaluate how well the channel environments are emulated. The chamber is considered to satisfy the far-field condition unless specifically stated. The probe panel covering 120° in the azimuth domain and 60° in the elevation domain is adopted. Three probe angular spacing cases, i.e., 3.75°, 7.5°, and 15°, are represented by θ_1, θ_2, and θ_3, respectively. The DUT rotation method maximizing the total power in probe coverage [37] is employed. The 3GPP 38.901 clustered delay line (CDL)-A, B, and C models are considered as the simulation channel [41]. Among these three channel models, the spatial angles of propagation paths are quite different. On the other hand, these three channels are with small, medium, and large angle spreads, respectively. Diverse channel characteristics can comprehensively validate the performance of our proposed methods.

A. Simulation Channels

1) Algorithm comparison: Taking the CDL-B channel emulation as an example, all the algorithm combinations are implemented with 12 probes in the θ_1 case. Fig. 2 shows the estimated PAS in the target environment, and the emulated PAS deviations estimated by DUT are shown in Fig. 3, where the white dots represent the cluster locations. The deviation is defined as the power difference between the target and the emulated PASs at each spatial angle of interest. For comparison, the power deviations are normalized to the maximum power of P_T. Obviously, compared to existing algorithms, the proposed methodologies significantly improve the emulation accuracy. As shown in Fig. 3. (a) and (b), though limited PAS similarity improvement is observed, the PAS deviations around the cluster locations are reduced in Fig. 3. (b), which is crucial

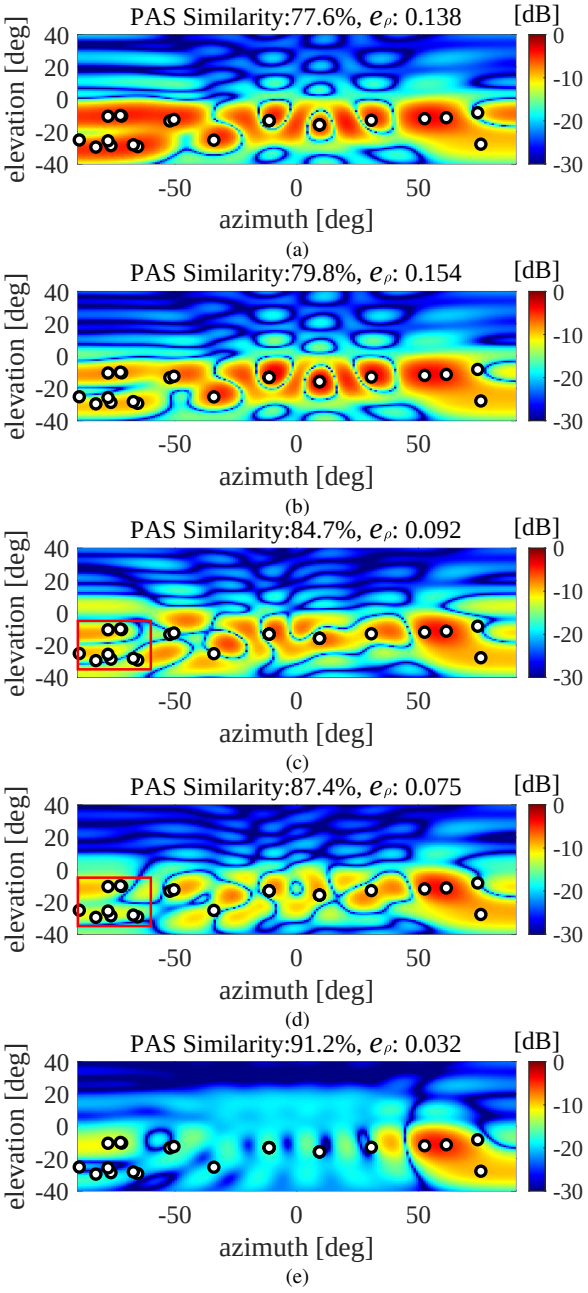

Fig. 3. The estimated PAS deviations between the emulated PAS and the target channel with the (a) B1, (b) B2, (c) B3, (d) B4, and (e) B5 algorithm combinations in the θ_1 case.

for the massive MIMO beamforming OTA testing, proving the advantage of the PAS reconstruction error-based probe weighting strategy. The performance degradation in spatial correlation emulation can be overcome by the advanced probe selection algorithm, as demonstrated in Fig. 3. (c), (d), and (e). Particularly, Fig. 4 shows the employed probe locations and weights with different algorithm configurations. There are two probes almost without power weights with the B2 algorithms, implying that these two probes hardly contribute to channel emulation, while all the probes selected with our proposed methods are excited about the emulation. On the other hand, as expected, the probes after adaptive correction are located around the probes selected with the OMP algorithm. Fig. 3. (d)

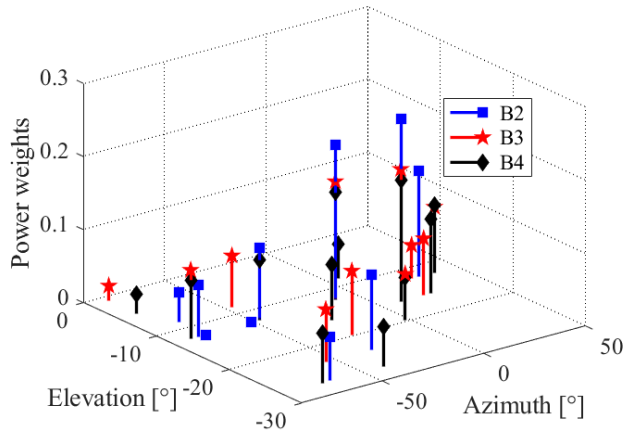

Fig. 4. The distributions of the probe locations obtained from different selection algorithms.

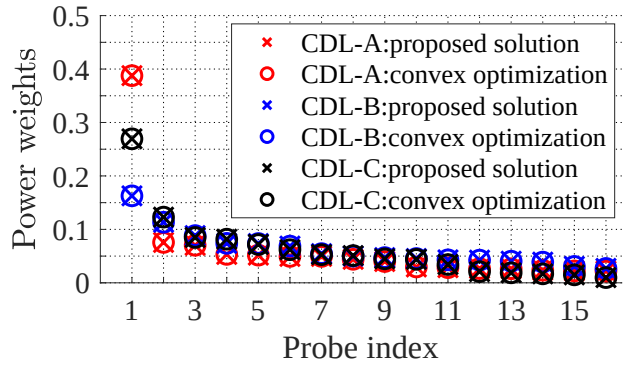

Fig. 5. The comparison of the probe weighs calculated with the proposed closed-form weighing method and the convex optimization methods for various channel models.

shows the performance improvement enabled by the proposed adaptive correction, especially in the red rectangle region, compared to the PAS emulated with the B3 configuration. It can be found that the performances provided by the proposed algorithms approach the performance upper bound presented in Fig. 3. (e).

2) Robustness and adaptability analysis: To demonstrate the accuracy of the proposed closed-form probe weighing strategy, Fig. 5 exhibits the power weights obtained from the proposed method and the convex optimization method for emulating the 3GPP CDL-A, B, and C channel models with 16 active probes. It can be seen that the proposed method provides identical solutions to that calculated from the convex optimization, enabling realistic channel reconstruction. In practice, convex optimization is, however, rather complicated and too time-consuming for multi-snapshot channel emulation.

Fig. 6-8 illustrate the performance metrics with different numbers of active probes in the θ_1 case for three representative channels emulated with various methodologies. For most scenarios, the proposed algorithms outperform the other configurations and offer satisfying emulation accuracy with different numbers of probes. However, marginal performance degradations with B4 can be observed in some cases, especially for the D_P and D_T. It is due to the fact that minimizing the mean PAS emulation error is not completely equivalent

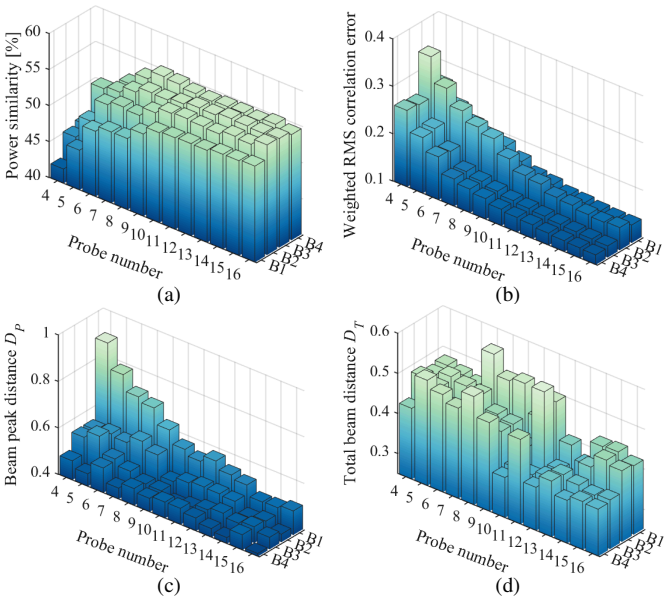

Fig. 6. Performance metrics with different probe numbers and algorithm configurations for CDL-A channel model emulation.

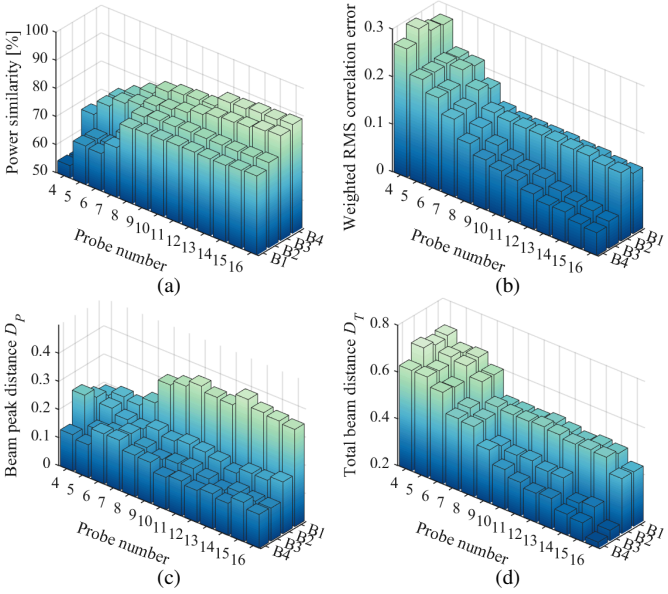

Fig. 7. Performance metrics with different probe numbers and algorithm configurations for CDL-B channel model emulation.

to minimizing the deviations for these metrics. Furthermore, these metrics are not completely related as well. For example, using the B5 configuration, the PAS similarity for CDL-A channel emulation is about 55.2%, but D_T is 0.4 higher than that obtained from the proposed methods with more than 8 active probes. Similar phenomena were found in [22]. Nevertheless, since the proposed adaptive correction procedure presents well adaptability, a novel correction criterion considering multi-dimensional characteristics can be developed for this problem, and it will be our future research.

In this section, the effects of chamber dimension and probe spacing on the effectiveness of our proposed algorithms are studied. According to the Fraunhofer criterion [23], the DUT requires a measurement distance of $5m$ for the far-field condition. Fig. 9 shows that even in near-field cases, the

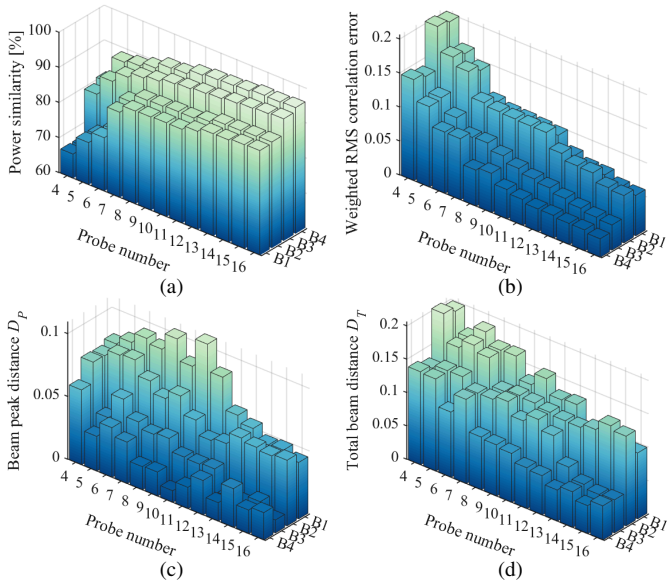

Fig. 8. Performance metrics with different probe numbers and algorithm configurations for CDL-C channel model emulation.

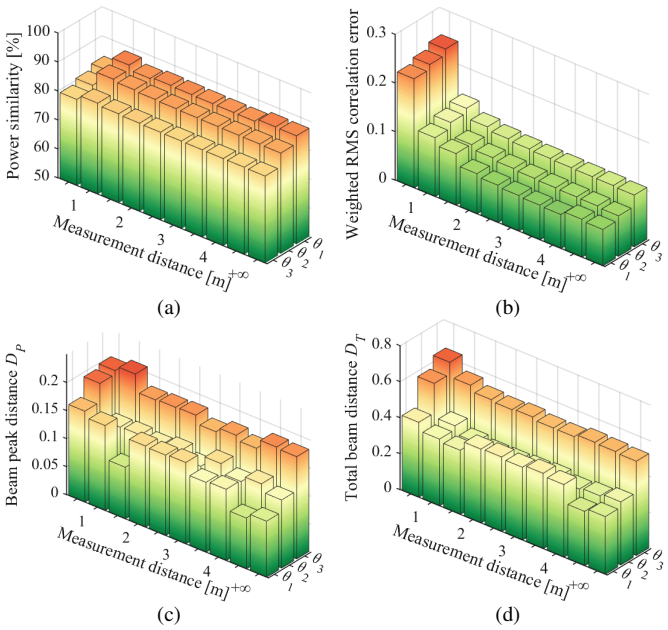

Fig. 9. Performance metrics with different measurement distances and probe spacing for CDL-B channel model emulation with 12 active probes and the B4 configuration.

proposed methods are capable of achieving similar results to that obtained in far-field cases. It indicates that the derived closed-form probe weighting strategy is practicable in near-field environments, and the effectiveness of equation (11) is demonstrated. The small performance variations are because the probe locations seen by the DUT change with different measurement distances.

3) Summary: Though marginal performance fluctuations exist, the proposed probe selection and weighting strategy can realize accurate channel emulation for the massive MIMO DUT testing and can be implemented computationally efficiently. To further enhance the accuracy and practicability, one of our future researches is a more reasonable criterion for the adaptive correction procedure. On the other hand, the selection region in adaptive correction can be restricted to accelerate the algorithm implementation.

B. Measured Channel Emulation

In addition to the well-defined 3GPP standard channels, the measured site or route-specific channel plays an essential role in the OTA testing as well since it provides a more realistic propagation environment for the DUT verification. An indoor measurement is introduced in the following, and the capacity of our proposed methodologies to reproduce the measured channel is validated.

1) Measurement campaign and channel characterization: An indoor measurement campaign at $2-4$ GHz was performed in the classroom of Aalborg University, Denmark. A vector network analyzer (VNA) based ultrawideband channel sounding system [42] with a virtual uniform circular array (UCA) is exploited to capture the non-stationary channel characteristics. Two biconical antennas, which are quasi-omnidirectional in the horizontal plane and have narrow radiation patterns in the elevation plane, are employed for the Tx and Rx sides. The measurement scenario and layout are shown in Fig. 10, where the three sides of the classroom are covered by concrete, and

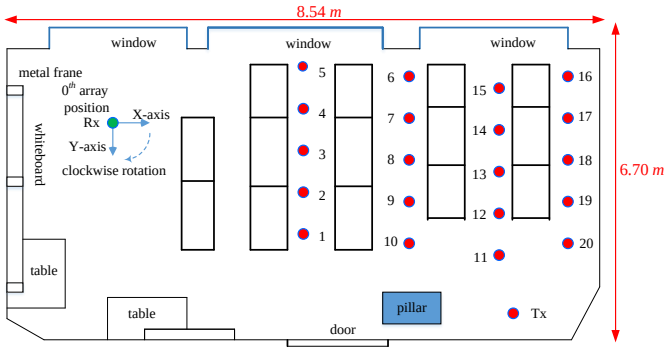

Fig. 10. The geometric layout of the measurement scenario.

three windows are on the other side. The dimension of the classroom environment is about $8.54 \times 6.70 \times 2.71\text{m}^3$. The Rx antenna was installed on a rotating pedestal with a preset radius of $r = 0.24$ m, and it was rotated clockwise in the azimuth plane with a 1 degree rotating step to form 360 UCA elements. Both heights of Tx and Rx antennas are 1.5 m. The height of the table is 0.74 m. Totally, there are 20 spatial snapshots (i.e., locations) that were measured in this scenario by sequentially moving the Tx with the spacing of 0.8 m. At each measurement location, the channel propagation between Tx and Rx was recorded using the VNA sweeping 750 points in the $2-4$ GHz frequency band. With the measured channel transfer functions (CTFs) at each measurement location, the multipath component (MPC) channel characteristics, including complex amplitudes, azimuth angles, elevation angles, and propagation delays, can be fully extracted by the high-resolution parameter estimation (HRPE) algorithm [43].

Fig. 11 illustrates the dynamic evolution of the MPC in the delay and azimuth domains over consecutive snapshots. Due to the narrow radiation pattern and the limited aperture of the

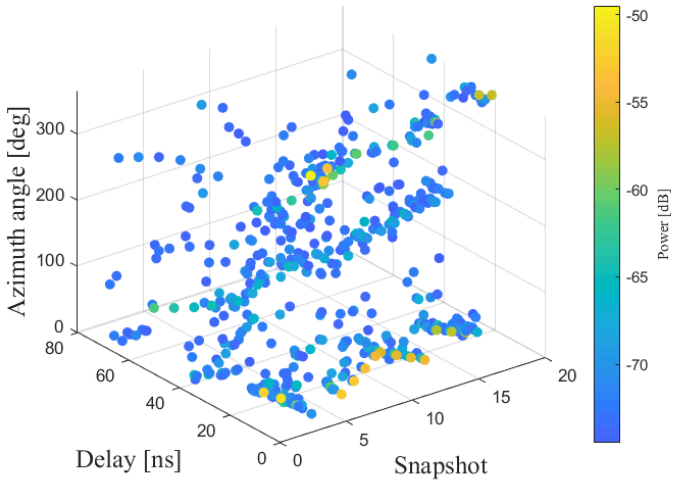

Fig. 11. The multi-snapshot environment characterization result.

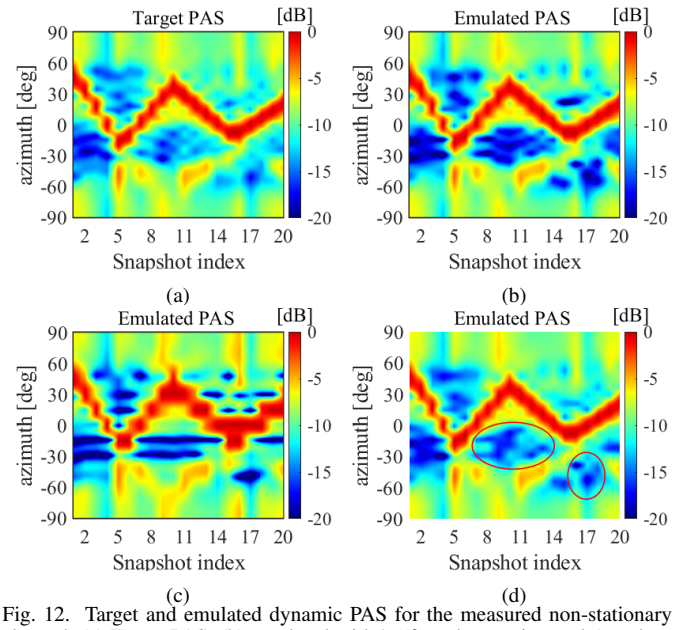

Fig. 12. Target and emulated dynamic PAS for the measured non-stationary channel. (a) Target PAS. (b) emulated with 7.5° probe spacing and 6 probes. (c) emulated with 15° probe spacing and 6 probes. (d) emulated with 7.5° probe spacing and 8 probes.

virtual UCA in elevation, only azimuth angles are taken into account. Different from the 3GPP standard channels, which are defined in cluster form, it can be observed that the MPCs of the measured channel are mixed, and the cluster boundaries among them are hard to be distinguished. It is problematic for the cluster-based probe selection algorithms, such as the widely used SAM method.

2) Emulation for the measured dynamic channel: Fig. 12 exhibits the measured channel PAS profile evolution behavior seen by the DUT sliced in the target and the emulated environments, where three types of probe configurations are employed in the SMPAC. Due to the large angular spread of the measured channel, a larger probe panel (covering 150° in azimuth) is adopted. The PAS power at each snapshot was normalized. Fig. 12. (c) shows that the emulated propagation trajectory is distorted with too large a probe spacing. Since the considered channel is quite directive due to the line-of-sight (LOS) path, a denser probe distribution is required. It has been concluded in [11] that the emulation performance will be detrimentally affected when the domain path is radiated from a direction far from the probe angles. It can be found in Fig. 12. (c) that the PAS emulated with 7.5° probe spacing presents satisfying fidelity with more than 95.6% PAS similarity. The trajectory of propagation evolution is consistent with the target. On the other hand, the main clusters are reproduced accurately, including the "birth-death" behaviors along the measurement route. More probes can be selected to further reproduce the PAS profiles of the weak clusters. As shown in Fig. 12. (d), using 8 active probes, more accurate PAS can be emulated, especially in the marked region, and the holistic PAS similarity of 97.2% and the weighted correlation error of no more than 0.1 can be obtained. Thus it can be concluded that the proposed probe selection algorithms present better applicability compared to SAM methods.

V. Conclusion

In this contribution, a novel SMPAC configuration solution is proposed for the performance evaluation of the massive MIMO device with beamforming mode, where realistic dynamic propagation environments can be accurately reproduced in an anechoic chamber by properly selecting and weighting the active probes. The comprehensive simulations for the 3GPP standard channel emulation indicate that the proposed closed-form probe weighting method based on minimizing the PAS reconstruction error significantly reduces the computational complexity without penalty on accuracy compared to that obtained with the complicated numerical algorithm. On the other hand, the proposed probe selection method further improves the channel emulation performances, and the robustness and adaptability are demonstrated with various SMPAC configurations. More importantly, the proposed probe selection algorithm is generic and does not rely on the cluster definition. To further validate the proposed algorithms, a measured non-stationary propagation (with a large dynamic range) is considered. The emulations for the realistic measured channel imply that the proposed methodologies are competent in efficiently reproducing the arbitrary channels and realizing the ergodic channel emulation.

References

[1] J. Zhang, Z. Zheng, Y. Zhang, J. Xi, X. Zhao, and G. Gui, "3D MIMO for 5G NR: Several observations from 32 to massive 256 antennas based on channel measurement," *IEEE Commun. Mag.*, vol. 56, no. 3, pp. 62–70, Mar. 2018.

[2] X. Zhao, A. M. A. Abdo, C. Xu, S. Geng, J. Zhang, and I. Memon, "Dimension reduction of channel correlation matrix using CUR-decomposition technique for 3-D massive antenna system," *IEEE Access*, vol. 6, pp. 3031–3039, Dec. 2017.

[3] E. G. Larsson, F. Tufvesson, O. Edfors, and T. L. Marzetta, "Massive MIMO for next generation wireless systems," *IEEE Commun. Mag., vol.*, vol. 52, no. 2, pp. 186–195, Feb. 2014.

[4] B. Yang, Z. Yu, J. Lan, R. Zhang, J. Zhou, and W. Hong, "Digital beamforming-based massive MIMO transceiver for 5G millimeter-wave communications," *IEEE Trans. Microw. Theory Techn.*, vol. 66, no. 7, pp. 3403–3418, Jul. 2018.

[5] A. F. Molisch *et al.*, "Hybrid beamforming for massive MIMO: A survey," *IEEE Commun. Mag.*, vol. 55, no. 9, pp. 134–141, Sep. 2017.

[6] Z. Pi and F. Khan, "An introduction to millimeter-wave mobile broadband systems," *IEEE Commun. Mag.*, vol. 49, no. 6, pp. 101–107, Jun. 2011.

[7] W. Roh *et al*., "Millimeter-wave beamforming as an enabling technology for 5G cellular communications: Theoretical feasibility and prototype results," *IEEE Commun. Mag.*, vol. 52, no. 2, pp. 106–113, Feb. 2014

[8] S. Rangan, T. Rappaport, and E. Erkip, "Millimeter-wave cellular wireless networks: Potentials and challenges," *Proc. IEEE*, vol. 102, no. 3, pp. 366–385, Mar. 2014.

[9] M. Xiao *et al*., "Millimeter wave communications for future mobile networks," *IEEE J. Select. Areas Commun.*, vol. 35, no. 9, pp. 1909–1935, Sep. 2017.

[10] W. Fan, X. Carreno Bautista de Lisbona, F. Sun, J. Ø. Nielsen, M. B. Knudsen, and G. F. Pedersen, "Emulating spatial characteristics of MIMO channels for OTA testing," *IEEE Trans. Antennas Propag.*, vol. 61, no. 8, pp. 4306–4314, Aug. 2013.

[11] W. Fan, P. Kyösti, M. Rumney, X. Chen and G. F. Pedersen, "Over the-air radiated testing of millimeter-wave beam-steerable devices in a cost-effective measurement setup," *IEEE Commun. Mag.*, vol. 56, no. 7, pp. 64–71, Jul. 2018.

[12] P. Shen, Y. Qi, W. Yu, F. Li, X. Wang and X. Shen, "A Directly Connected OTA Measurement for Performance Evaluation of 5G Adaptive Beamforming Terminals," *IEEE Internet Things J.*, vol. 9, no. 16, pp. 15362-15371, Aug. 2022

[13] P. Kyösti, T. Jämsä, and J.-P. Nuutinen, "Channel modelling for multiprobe over-the-air MIMO testing," *International Journal of Antennas and Propagation*, vol. 2012, Art. no. 615954, Mar. 2012.

[14] P. Shen, Y. Qi, W. Yu, J. Fan, and F. Li, "OTA measurement for IoT wireless device performance evaluation: Challenges and solutions," *IEEE Internet Things J.*, vol. 6, no. 1, pp. 1223–1237, Feb. 2019.

[15] Y. Li, L. Xin, X. Liu, and X. Zhang, "Dual anechoic chamber setup for overthe-air radiated testing of 5G devices," *IEEE Trans. Antennas Propag.*, vol. 68, no. 3, pp. 2469–2474, Mar. 2020.

[16] Z. Jiang, Z. Wang, C. Guo, Z. -C. Hao and W. Hong, "Time-Domain Nonstationary Channel Emulation in Multiprobe Anechoic Chamber Setups for Over-the-Air Testing," *IEEE Antennas Wireless Propag. Lett.*, vol. 20, no. 12, pp. 2511-2515, Dec. 2021.

[17] "Test Plan for 2 × 2 Downlink MIMO and Transmit Diversity Over-the-Air Performance," CTIA Certification, CTIA, Washington, DC, USA, Version 1.1.1, Sep. 2017.

[18] 3GPP TR 38.827, "Study on Radiated Metrics and Test Methodology for the Verification of Multi-Antenna Reception Performance of NR User Equipment (UE)," v. 16.4.0, Oct. 2021.

[19] W. Fan, F. Zhang, and Z. Wang, "Over-the-air testing of 5G communication systems: Validation of the test environment in simple-sectored multiprobe anechoic chamber setups," *IEEE Antennas Propag. Mag.*, vol. 63, no. 1, pp. 40–50, Oct. 2019.

[20] H. Gao *et al*., "Over-the-Air Performance Testing of 5G New Radio User Equipment: Standardization and Challenges," *IEEE Communications Standards Magazine*, vol. 6, no. 2, pp. 71-78, Jun. 2022.

[21] P. Kyösti, L. Hentilä, J. Kyröläinen, F. Zhang, W. Fan, and M. Latvaaho, "Emulating dynamic radio channels for radiated testing of massive MIMO devices," in *Proc. 12th Eur. Conf. Antennas Propag. (EuCAP)*, Apr. 2018, pp. 1–5.

[22] P. Kyösti, L. Hentilä, W. Fan, J. Lehtomäki, and M. Latva-Aho, "On radiated performance evaluation of massive MIMO devices in multiprobe anechoic chamber OTA setups," *IEEE Trans. Antennas Propag.*, vol. 66, no. 10, pp. 5485–5497, Oct. 2018.

[23] P. Kyösti, W. Fan, G. F. Pedersen, and M. Latva-aho, "On dimensions of OTA setups for massive MIMO base stations radiated testing," *IEEE Access*, vol. 4, pp. 5971–5981, Sep. 2016.

[24] U. T. Virk, L. Hentilä, P. Kyösti and J. Kyröläinen, "Validating FR2 MIMO OTA Channel Models in 3D MPAC," in *Proc. 16th Eur. Conf. Antennas Propag. (EuCAP)*, Apr. 2022, pp. 1–5.

[25] X. Cai, Y. Miao, J. Li, F. Tufvesson, G. F. Pedersen and W. Fan, "Dynamic mmWave Channel Emulation in a Cost-Effective MPAC With Dominant-Cluster Concept,"*IEEE Trans. Antennas Propag.*, vol. 70, no. 6, pp. 4691-4704, Jun. 2022.

[26] Y. Ji and W. Fan, "Enabling High-Fidelity Ultra-Wideband Radio Channel Emulation: Band-Stitching and Digital Predistortion Concepts," *IEEE Open Journal of Antennas and Propagation*, vol. 3, pp. 932-939, Aug. 2022.

[27] H. Pei, X. Chen, W. Xue, M. Zhang, and T. Svensson, "Impact of probe coupling on emulation accuracy in massive MIMO OTA testing," in *Proc. 14th Eur. Conf. Antennas Propag. (EuCAP)*, Mar. 2020, pp. 1–4.

[28] H. Wang *et al*., "On Efficient Non-Stationary Channel Emulation in Conductive Phase Matrix Setup for Massive MIMO Performance Testing,"*IEEE Trans. Veh. Technol.*, vol. 71, no. 8, pp. 8030-8041, Aug. 2022

[29] H. Pei *et al*., "Key issues and algorithms of multiple-input-multipleoutput over-the-air testing in the multi-probe anechoic chamber setup," *Sci. China Inf. Sci*., vol. 65, no. 3, 2022, Art. no. 131302.

[30] D. Fan *et al*., "Angle domain channel estimation in hybrid millimeter wave massive MIMO systems,"*IEEE Trans. Wireless Commun.*, vol. 17, no. 12, pp. 8165–8179, Dec. 2018.

[31] H. Wang, W. Wang, H. Gao, Y. Wu, Y. Liu, and J. Gao, "Plane wave compensation technique for multiple-input multiple-output over-the-air testing in small multi-probe anechoic chamber," *IET Microw., Antennas Propag.*, vol. 13, no. 15, pp. 2625–2631, Dec. 2019.

[32] W. Fan, F. Sun, J. Ø. Nielsen, X. Carreo, J. S. Ashta, M. B. Knudsen, and G. F. Pedersen, "Probe selection in multi-probe OTA setups," *IEEE Trans. Antennas Propag.*, vol. 62, no. 4, pp. 2109–2120, Apr. 2014.

[33] Y. Li, L. Xin, and X. Zhang, "On probe weighting for massive MIMO OTA testing based on angular spectrum similarity,"*IEEE Antennas Wireless Propag. Lett.*, vol. 18, no. 7, pp. 1497–1501, Jul. 2019.

[34] W. Fan, L. Hentilä, F. Zhang, P. Kyösti, and G. F. Pedersen, "Virtual drive testing of adaptive antenna systems in dynamic propagation scenarios for vehicle communications," *IEEE Access*, vol. 6, pp. 7829–7838, Jan. 2018.

[35] P. Bello, "Characterization of randomly time-variant linear channels," *IEEE Trans. Commun.*, vol. 11, no. 4, pp. 360–393, Dec. 1963.

[36] W. Fan *et al*, "3D channel emulation in multi-probe setup," *Electron. Lett.*, vol. 49, no. 9, pp. 623–625, Apr. 2013.

[37] H. Wang, W. Wang, Y. Wu, B. Tang, W. Zhang, and Y. Liu, "Probe selection for 5G massive MIMO base station over-the-air testing," *IEEE Antennas Wireless Propag. Lett.*, vol. 19, no. 11, pp. 1998–2002, Nov. 2020.

[38] G. Davis, S. Mallat, and M. Avellaneda, "Adaptive greedy approximations," *J. Constructive Approximation*, vol. 13, no. 1, pp. 57–98, 1997.

[39] P. Stoica and R. L. Moses, *Spectral analysis of signals*. Pearson/Prentice Hall Upper Saddle River, NJ, 2005.

[40] S. Boyd and L. Vandenberghe, *Convex Optimization*. Cambridge, U.K.: Cambridge Univ. Press, 2004

[41] *Study on Channel Model for Frequencies From 0.5 to 100 GHz*, document TR 38.901, Revision 14.2.0, 3GPP, Sep. 2017.

[42] G. Zhang, K. Saito, W. Fan, X. Cai, P. Hanpinitsak, J.-I. Takada, and G. F. Pedersen, "Experimental characterization of millimeter-wave indoor propagation channels at 28 GHz," *IEEE Access*, vol. 6, pp. 76516–76526, Nov. 2018.

[43] X. Cai and W. Fan, "A complexity-effificient high resolution propagation parameter estimation algorithm for ultra-wideband large-scale uniform circular array," *IEEE Trans. Commun.*, vol. 67, no. 8, pp. 5862–5874, Aug. 2019.